等离子喷涂及真空热处理过程中 $MoSi_2$ 涂层的相演变

颜建辉[1,2]， 张厚安[2]， 李益民[1]， 唐思文[2]
（1. 中南大学 粉末冶金国家重点实验室，长沙 410083；
2. 湖南科技大学 先进材料制备及应用技术研究所，湖南 湘潭 411201）

摘 要：分别采用 $MoSi_2$，Mo-66.7%Si 和 Mo-70%Si（摩尔分数）粉末为原料，在 45 钢上大气等离子喷涂 $MoSi_2$ 涂层，对喷涂前后相以及真空热处理对涂层相和组织的影响进行了研究。结果表明，以 $MoSi_2$ 为原料喷涂后，涂层主要是由 $MoSi_2$ 和 Mo_5Si_3 相组成，$MoSi_2$ 由亚稳定的 $MoSi_2$(h) 六方结构和稳定的 $MoSi_2$(t) 四方晶体结构组成。而 Mo-66.7%Si 和 Mo-70%Si 两种粉末喷涂后，涂层均由 Mo，Si 单质粉组成，喷涂过程没有形成硅化物。Mo-66.7%Si 涂层在 1 050，1 200 ℃热处理 1 h 后，涂层中主相是 Mo_5Si_3，次相为 $MoSi_2$。Mo-70%Si 涂层在 800，1 000 ℃热处理 30 min 后，生成了少量的 $MoSi_2$，Mo_5Si_3 和 Mo_3Si。在 1 050 ℃热处理时，随着时间的延长，$MoSi_2$ 相含量相对增多，当热处理时间为 30，45 min 时，由于 Mo，Si 和 Fe 之间的反应扩散，还生成了 FeMoSi 和 Fe_3Si 相。

关键词：等离子喷涂；真空热处理；$MoSi_2$ 涂层；相演变
中图分类号：TQ174.5 文献标识码：A 文章编号：0253－360X(2008)08－0032－05

颜建辉

0 序 言

金属间化合物 $MoSi_2$ 具有高熔点（2 030 ℃）、低密度（6.24×10^3 kg/m^3）、良好的导热性和导电性以及优良的高温抗氧化能力而成为最有希望的结构材料之一[1]。由于高温下 $MoSi_2$ 氧化生成具有保护性质的致密 SiO_2 膜，所以 $MoSi_2$ 用于难熔金属及其合金和 C/C 复合材料的高温抗氧化涂层是目前研究的热点之一[2,3]。采用料浆烧结法、包埋法、气相沉积法、熔盐法和激光熔覆技术等方法制备出了 $MoSi_2$ 及其复合材料涂层，涂层与基体材料达到较好的冶金结合，表现出较好的抗热震性能和好的高温抗氧化性能[4－7]。然而，采用等离子喷涂技术，涂层成分可在较大范围内变化，涂层厚度容易控制且操作方便。

金属间化合物 $MoSi_2$ 具有优越的耐磨性能，有望成为特殊领域工况下选用的新型耐磨零部件[8,9]。用作涂层，可望改善钢铁的抗磨性能。以 $MoSi_2$ 作为涂层体系，采用大气等离子喷涂法在 45 钢上制备 $MoSi_2$ 涂层，重点研究了不同类型的粉末喷涂后的相组成，以及真空热处理对涂层的相、组织形貌的影响，为 $MoSi_2$ 涂层的应用提供试验数据和经验。

收稿日期：2007－10－20
基金项目：国家自然科学基金资助项目（50405041）

1 试验方法

试验基体材料选用 45 钢，试样尺寸为 18 mm×12 mm×5 mm，喷涂前，先对试样表面进行除油和去锈、然后对试样进行喷砂处理，使试样表面具有一定的粗糙度，用超声波清洗仪清洗试样表面，干燥后待用。

用钼和硅粉采用高温自蔓延合成技术制备 $MoSi_2$ 粉末。同时，将钼、硅单质粉按 Mo-66.7%Si 和 Mo-70%Si（摩尔分数）原子配比均匀混合上述两种粉末。以 $MoSi_2$，Mo-66.7%Si 和 Mo-70%Si 粉末为原料，采用 APS－2000 型大气等离子喷涂设备制备 $MoSi_2$ 涂层。并对 Mo-66.7%Si 和 Mo-70%Si 粉末制备的涂层在不同温度和时间下进行真空热处理并随炉冷却。

用德国 D8－Advance 型全自动 X 射线衍射仪检测粉末和涂层的物相组成，采用 KYKY2800 和

JSM—5100LV 扫描电镜来观察涂层的表面和截面形貌。

2　试验结果及讨论

2.1　$MoSi_2$ 粉末

图 1 为自蔓延高温合成的 $MoSi_2$ 粉末 SEM 形貌，$MoSi_2$ 为不规则的颗粒状，粉末平均粒径 10 μm。XRD（图 2）分析表明，$MoSi_2$ 粉末主要由 $MoSi_2$ 组成，结构为 C11b 型四方晶体结构，还有极少量的残留单质钼相。

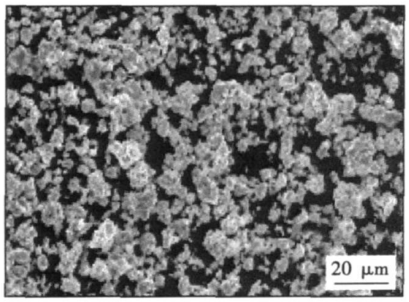

图 1　$MoSi_2$ 粉末 SEM 形貌

Fig. 1　SEM microstrucure of $MoSi_2$ powder

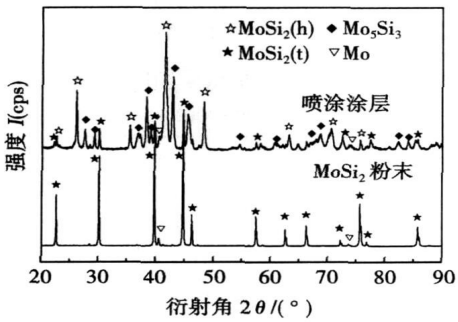

图 2　$MoSi_2$ 原始粉末和喷涂态衍射图

Fig. 2　XRD pattern of raw and sprayed $MoSi_2$

2.2　$MoSi_2$ 粉末制备涂层的相组成和组织

图 2 为 $MoSi_2$ 粉末等离子喷涂制备涂层的衍射结果。可知，用 $MoSi_2$ 粉末制备的涂层的相组成与原始 $MoSi_2$ 粉末的相存在很大的不同。喷涂态涂层主要由 $MoSi_2$ 和 Mo_5Si_3 组成，还有少量的钼相。原始粉末的 $MoSi_2$ 相是属于稳定的 C11b 型 $MoSi_2$（t）四方晶体结构，由于等离子喷涂火焰温度非常高，喷涂过程中，熔融 $MoSi_2$ 全部是 $MoSi_2$（h）结构（1 900 ℃以上为不稳定的相），由于快速冷却，等离子喷涂冷却过程中不稳定 $MoSi_2$（h）六方结构部分转变为稳定的 C11b 型 $MoSi_2$（t）四方晶体结构。

图 3a 为涂层的表面形貌。由于高速喷射 $MoSi_2$ 熔滴对基体表面的碰撞，熔滴因动能的冲击压力而变形、润湿、铺展，最后凝固冷却形成薄饼状的变形颗粒。变形颗粒的尺寸、变形程度和分布是比较均匀的。从图片可以看出，$MoSi_2$ 涂层的表面可以大致分为完全熔融和未完全熔融两部分。未熔融的部分，涂层致密性较差，颗粒保持原有颗粒的特征，多

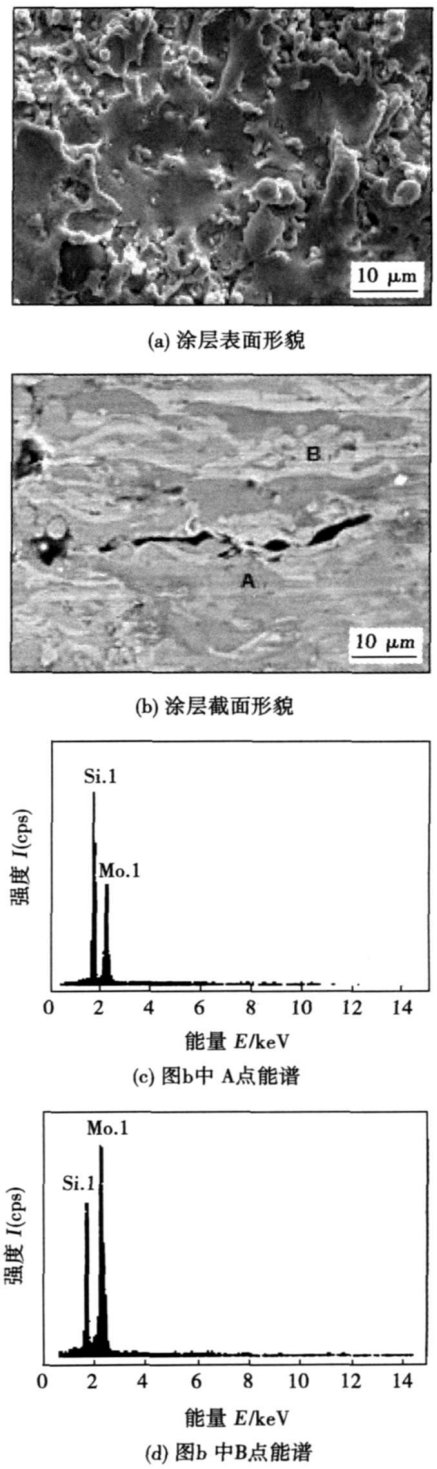

图 3　$MoSi_2$ 粉末制备的涂层

Fig. 3　Coating of $MoSi_2$ prepared raw material

个颗粒堆积在一起，颗粒间具有明显的界面，是由于少数颗粒熔解不充分或熔解后又凝固，导致少数颗粒呈为球形状。而熔融部分的表面光滑成薄饼状，致密性较好。

图3b为涂层截面组织背散射图。可见，涂层截面为典型的层状结构。在$MoSi_2$涂层的片层颗粒与片层颗粒之间还存在层间薄的气隙。这层孔隙，平行于熔滴的变形方向，呈“扁形”。这种层状孔隙，显著地弱化了$MoSi_2$片层与片层之间的粘结性能。图3b的区域(A，B点)能谱(EDS)如图3c，d所示。可知，深色相A点Mo/Si原子比接近1∶2，而浅白色相B点Mo/Si原子比接近5∶3。结合衍射图谱(图2)可知，深色相和浅白色相分别为$MoSi_2$和Mo_5Si_3，两种相之间存在明显的界面。

大气等离子喷涂过程中，熔融颗粒尽管有氩气和氢气保护，但还是会被卷入氧气。在$MoSi_2$涂层中，Si优先氧化形成非晶态SiO_2，在喷涂过程中SiO_2易氧化挥发(熔点和沸点分别为1 625，2 230 ℃)，导致大量的硅损失，从而形成富钼相或单质钼。在大气等离子喷涂过程中，熔融的$MoSi_2$可能发生如下反应

$$5MoSi_2(s)+7O_2 \rightarrow Mo_5Si_3(s)+7SiO_2(g)$$

$$5MoSi_2(s)+2O_2 \rightarrow Mo(s)+2SiO_2(g)$$

$$2MoSi_2(s)+7O_2 \rightarrow 2MoO_3(g)+4SiO_2(g)$$

文献[10]在大气等离子喷涂Mo-13.4Si-2.6B粉末时，发现以180，350 m/s的速度喷涂时，原粉末中的硅损失分别为56%和14%，并且也生成了Mo_5Si_3和单质钼，与文中研究结果相似。

2.3 Mo-66.7%Si涂层热处理

图4为Mo-66.7%Si粉末喷涂态和该涂层真空热处理后(1 050 ℃×45 min和1 200 ℃×60 min)的衍射结果。Mo-66.7%Si单质混合粉末在热喷涂过程中未原位合成$MoSi_2$，还是以Mo，Si单质元素存在。

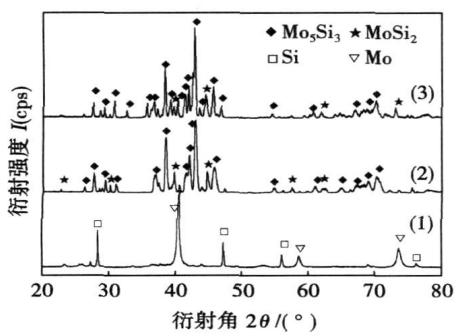

(1)喷涂态；(2)1 050 ℃×60 min；(3)1 200 ℃×60 min

图4 Mo-66.7%Si涂层热处理衍射图

Fig. 4 XRD pattern of Mo-66.7mol% Si sprayed and thermal treated coating

但经过热处理后，钼和硅反应合成了Mo_5Si_3和Mo_5i_2相，基本上没有Mo和Si单质元素存在。硅的熔点是1 410 ℃，沸点是2 355 ℃，钼的熔点是2 610 ℃，沸点是5 560 ℃。在热喷涂过程中损失了部分硅，导致热处理时不能完全生成$MoSi_2$，还含有大量的Mo_5Si_3富钼相。

Mo-66.7%Si涂层1 050 ℃真空热处理45 min后的截面扫描如图5所示。涂层三个不同颜色的区域能谱分析结果见表1。可知，A点主要是$MoSi_2$，B点主要是Mo_5Si_3，而C区域是铁、钼和硅组成的物质。结合衍射结果知道，涂层外层主要是$MoSi_2$和Mo_5Si_3相。在涂层和钢基体界面处Fe，Mo和Si元素发生了扩散反应，形成的化合物有利于提高涂层与基体材料的结合强度。

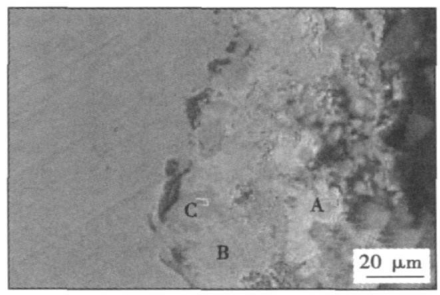

图5 Mo-66.7%Si涂层截面

Fig. 5 Sectional morphology of Mo-66.7mol% Si coating

表1 图5能谱分析结果(摩尔分数，%)

Table 1 EDS of different points in Fig. 5

	Mo	Si	Fe
A	32.1	67.9	0
B	65.6	33.98	0.42
C	30.46	23.86	45.67

2.4 Mo-70%Si涂层热处理

图6为Mo-70%Si粉末喷涂后在不同温度和不

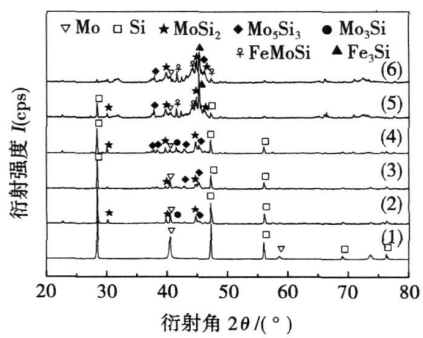

(1)喷涂态；(2)800 ℃×30 min；(3)1 000 ℃×30 min；(4)1 050 ℃×10 min；(5)1 050 ℃×30 min；(6)1 050 ℃×45 min

图6 Mo-70%Si涂层热处理衍射图

Fig. 6 XRD pattern of Mo-70mol% Si sprayed and thermal treated coating

同时间热处理后的衍射图。可知,Mo-70%Si 喷涂后仍然是以 Mo,Si 单质元素的形式存在。在800 ℃和 1 000 ℃热处理 30 min 后,生成了少量的 $MoSi_2$,Mo_5Si_3 和 Mo_3Si。在1 050 ℃热处理时,随着时间的延长,Mo_3Si 相逐渐消失,$MoSi_2$ 含量相对增多,在热处理 30,45 min时,由于钼、硅和铁之间的扩散,还生成了 FeMoSi 和 Fe_3Si 相。

Mo-70%Si 涂层的喷涂态横截面如图 7a 所示,涂层约为10 μm。1 050 ℃真空热处理45 min后的截面扫描图见 7b,涂层与界面出现了部分裂纹,该涂层两个不同颜色的区域能谱如图 7c,d。A 点主要是铁和硅的化合物,而 B 点主要是 Fe,Si,Mo 三个元

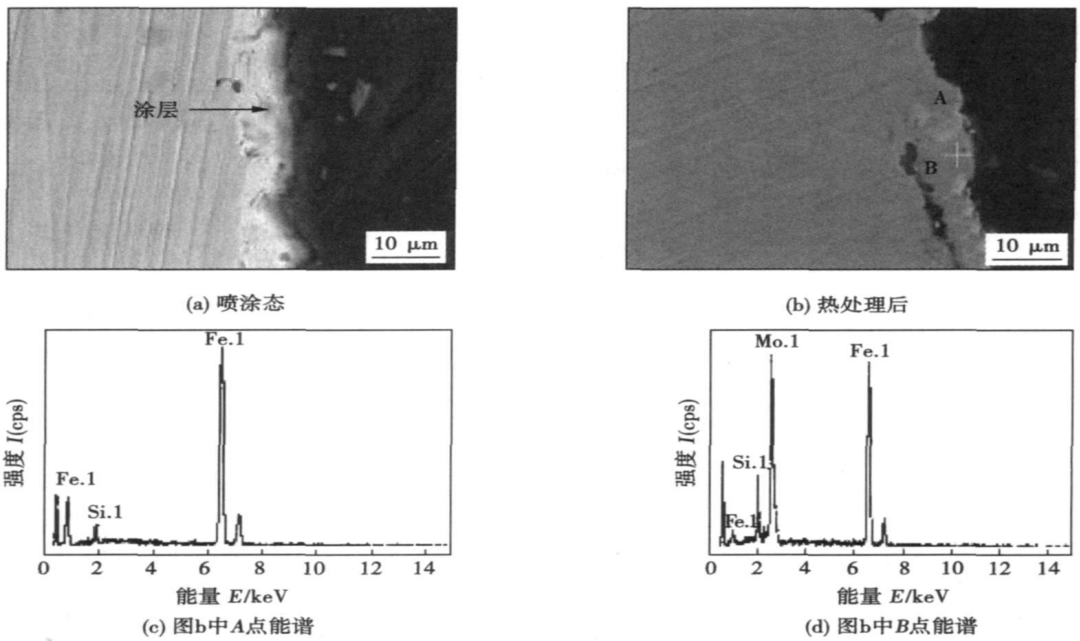

图 7　Mo-70%Si 粉末制备的涂层截面

Fig. 7　Coating of Mo-70 mol%Si prepared raw material

素组成的物质。结合图 6 衍射结果可知,A 区域是 Fe_3Si,而 *B* 点 FeMoSi,$MoSi_2$ 和 Mo_5Si_3 混合的物质。在 Fe-Si 系统中,铁在 Fe_3Si 相中的扩散是最快的,铁和硅最容易形成 Fe_3Si[7],所以其衍射峰强度最高。

3　结　　论

(1) $MoSi_2$ 粉末经过大气等离子喷涂后主要由 $MoSi_2$ 和 Mo_5Si_3 相组成,同时还有少量的钼相。原始粉末的 $MoSi_2$ 相是属于稳定的 C11b 型 $MoSi_2$(t)四方晶体结构,涂层由不稳定 $MoSi_2$(h)六方结构和稳定的 $MoSi_2$(t)四方晶体结构组成。

(2) Mo-66.7%Si 粉末制备的涂层由 Mo 和 Si 单质元素组成。Mo-66.7%Si 涂层1 050 ℃真空热处理 45 min后,表层主要是 $MoSi_2$ 和 Mo_5Si_3 相。而涂层和钢基体的界面处是由铁、钼和硅扩散反应生成的化合物。

(3) Mo-70%Si 粉末喷涂涂层是以Mo 和Si 单质元素的形式存在。在 800,1 000 ℃热处理30 min后,生成了少量的 $MoSi_2$,Mo_5Si_3和 Mo_3Si 相。在1 050 ℃热处理时,随着时间的延长,$MoSi_2$ 相含量相对增多。在热处理 30,45 min 时,还生成了 FeMoSi 和 Fe_3Si 相。

参考文献:

[1] Petrovic J J. Key development in high temperature structural silicides materials[J]. Materials Science Engineering A, 1999, 261: 1—5.

[2] Federico Smeacetto, Monica Ferraris, Milena Salvo. Multilayer coating with self-sealing properties for cebon-carbon composites[J]. Carbon, 2003, 41: 2105—2111.

[3] Nomura N, Suzuki T, Yoshimi K, *et al*. Microstrure and oxidation resistance of a plasma sprayed Mo-Si-B multiphase alloy caoting[J]. Intermetallics, 2003, 11: 735—742.

[4] 肖来荣, 蔡志刚, 宋　成. Mo(Si, A1)$_2$ 高温抗氧化涂层的形貌与结构研究[J]. 兵器材料科学与工程, 2006, 29(3): 50—53.

[5] 冉丽萍, 易茂中, 蒋建献, 等. 碳/碳复合材料 $MoSi_2$/SiC 高温抗氧化复合涂层的制备及其结构[J]. 新型炭材料, 2006, 21(9): 231－236.

[6] 徐子文, 阮中键. 激光熔覆 Mo-Si 难熔金属硅化物高温涂层的加工工艺、组织与性能[J]. 耐火材料, 2003, 37(1): 34－37.

[7] Ryosuke O, Suzuki masayori Ishikawa, Katsutoshi Ono. $MoSi_2$ coating on molybdenum using molten salt[J]. Journal of Alloys and Compounds, 2000(306): 285－291.

[8] Hawk J A, Alman D E. A comparative study of the abrasive wear behavior of $MoSi_2$[J]. Scripta Metallurgica et Materialia, 1995, 32(5): 725－729.

[9] 胡小平, 张厚安, 颜建辉, 等. 油润滑下 $MoSi_2$ 材料的摩擦磨损性能[J]. 中国机械工程, 2006, 17(15): 1630－1634.

[10] Terry C. Totemeier, Richard N, *et al*. FeAl and Mo-Si-B intermetallic coatings prepared by thermal spraying[J]. Intermetallics, 2004, 12: 1335－1344.

作者简介: 颜建辉, 男, 1973 年出生, 讲师, 博士研究生。主要从事高温结构材料制备、性能及抗氧化耐磨涂层方面的教学科研工作。发表论文 28 篇。

Email: yanjianhui88@163.com

[上接第 28 页]

(3) La^{3+} 离子掺杂引起 TiO_2 紫外—可见吸收光谱发生红移, 增加了 TiO_2 光激发波长范围。

(4) La^{3+} 离子掺杂能显著提高 TiO_2 的光催化活性, 最佳掺杂浓度为 0.5%(与 Ti 原子摩尔比), 甲基橙降解率在 90 min 内可达到 82.4%。

参考文献:

[1] Litter M I, Navio J A. Photocatalytic properties of iron-doped titania semiconductors[J]. Journal of Photochemistry and Photobiology A: Chemistry, 1996, 98: 171－181.

[2] Kanazawa T, Ohmori A. Behavior of coating formation on PET plate by plasma spraying and evaluation of coating's photocatalytic activity [J]. Surface and Coatings Technology, 2005, 197: 45－50.

[3] Araña J. Maleic acid photocatalytic degradation using Fe-TiO_2 catalysts dependence of the degradation mechanism on the Fe catalysts content[J]. Applied Catalysis B: Environmental, 2002, 36: 113－124.

[4] Miki-Yoshida M, Collins-Martinez V, Amezaga-Madrid P, *et al*. Thin films of photoca-talytic TiO_2 and ZnO deposited inside a tubing by spray pyrolysis[J]. Thin Solid Films, 2002, 419: 60－64.

[5] Trapalis C C, Keivanidis P, kordas G, *et al*. TiO_2 (Fe^{3+}) nanostructured thin films with antibacterial properties[J]. Thin Solid Film, 2003, 433: 186－190.

[6] 陈崧哲, 徐盛明, 徐 刚. 稀土元素在光催化剂中的应用及作用机理[J]. 稀有金属材料工, 2006, 35(4): 505－509.

[7] 高 濂, 张青红, 郑 珊. 纳米二氧化钛光催化材料及应用[M]. 北京: 化学工业出版社, 2002.

[8] 周 玉. 材料分析方法[M]. 北京: 机械工业出版社, 2003.

[9] 跃林海, 水 淼. 稀土掺杂二氧化钛的相变和光催化活性[J]. 浙江大学学报, 2000, 27(1), 69－73.

[10] 刘保顺, 何 鑫, 赵修建. 纳米 TiO_2 的表面能态及光生电子—空穴对复合过程的研究[J]. 光谱学与光谱分析, 2006, 26(2): 209－210.

[11] 刘守新, 刘 鸿. 光催化及光电催化基础与应用[M]. 北京: 化学工业出版社, 2006.

作者简介: 雷阿利, 女, 1957 年出生, 副教授。主要从事材料的加工与材料的腐蚀与防护方面的教学和科研工作。发表论文 30 余篇。

Email: leiali@126.com

cy filtering; image processing

Numerical analysis on N_2-Ar plasma welding arc LEI Yucheng, WANG Jian, ZHU Bin (School of Materials Science and Engineering, Jiangsu University, Zhenjiang, Jiangsu 212013, China). p17—20

Abstract: Aimed at Ar-N_2 plasma welding arc, a mathematic model was established according to the theory of magnetic fluid dynamics. PA welding arc was numerically analyzed by the 3D, static and axisymmetric model with ANSYS software. The temperature, electromagnetic force and velocity profiles of the Ar-N_2 protecting arc have been simulated. The characteristic of the Ar-N_2 protecting plasma welding arc was analyzed and compared with the Ar protecting plasma arc. The results show that with the mixed plasma gas the maximum temperature of the arc is higher than that of the Ar plasma arc. And the maximum temperature area leans to the anode.

Key words: PAW welding arc; magnetic fluid dynamics; numerical analysis

High-chromium iron-base composite coating prepared by reactive plasma cladding using asphalt as carbonaceous precursor LIU Junbo, LIU Aiping (School of Mechanical and Electronic Engineering, Weifang University, Weifang, Shandong 261061, China). p21—24

Abstract: A kind of Fe-Cr-C-W-Ni composite powders for reactive plasma cladding was prepared using iron, chromium, wolframium, nickel and sucrose (to pyrolyze the sucrose as carbonaceous precursor) as raw materials. High-chromium iron-base composite coatings were synthesized on the hardened and tempered C grade steel by reactive plasma cladding. Results show that the particle of Fe-Cr-C-W-Ni composites powder for cladding is uniform without any impurity. The high-chromium iron-base composite coating by reactive plasma cladding consists of a lot of the primary reinforced phase of $(Cr, Fe)_7C_3$ which distributes on the matrix of eutectic $(Cr, Fe)_7C_3/\gamma$. The coating has a metallurgical bonding with hardened and the substrate of tempered C grade steel. The average microhardness of the coating is about 1 100 HV. Under the same condition of wear test, the wear volume of the high-chromium iron-base composite coating is one seventh of that of the Ni60 coating by reactive plasma cladding.

Key words: reactive plasma cladding; high-chromium iron-base; precursor; composite coating

Characterization of La^{3+} doped TiO_2 prepared by plasma spraying LEI Ali, XU Dapeng, FENG Lajun, ZHU Guang, LI Gaohong (School of Material Science and Engineering, Xi'an University of Technology, Xi'an, 710048, China). p25—28

Abstract: TiO_2 nanopowders doped by the lanthanum trivalent ion were prepared by plasma thermal spray with solution of titanium tetra-tert-butoxide. And TiO_2 were characterized by XRD, XPS TEM and UV-Vis. The photocatalytic activities were also investigated. The results showed that the prepared doped powders are the mixture structure of anatase and rutile. La^{3+} doping can promote the transformation of TiO_2 from anatase to rutile, at the same time, it can restrain TiO_2 particle growing up. La^{3+} doping greatly increases the photocatalytic activity of TiO_2, the optimal doping concentration was 0.5%, and the degradation rate of methyl orange is 82.4%, which is 13.2% higher than that with pure TiO_2.

Key words: TiO_2; plasma spray; doping; La^{3+}

Numerical simulation on weld formation of twin-electrode GTAW welding ZHANG Guangjun, ZHAO Linlin, LENG Xuesong (State Key laboratory of Advanced Welding Production Technology, Harbin Institute of Technology, Harbin 150001, China). p29—31

Abstract: The weld formation of twin-electrode tungsten inert gas (T-TIG) welding was studied with numerical simulation. With a view to the arc deflection from the mutual attraction between the two arcs, inclined heat source model was adopted. The weld formation features of T-TIG and traditional TIG were comparatively analyzed. The effects of electrode distance, the current value and the matching of currents on the shape of melting pool were studied. The results show that compared with single-electrode tungsten inert gas, the weld width of T-TIG is narrower, and the weld depth is little smaller; with the increasing of electrode distance, the weld width increases, the weld depth decreases; With the increase of currents, the weld depth and width both increase; the current matching forms between electrodes also have certain influences on the weld formation.

Key words: twin-electrode tungsten inert gas welding; weld formation; numerical simulation; temperature field

Phases evolution of molybnenum silicide coating in plasma spraying and heat treatment process YAN Jianhui[1,2], ZHANG Houan[2], LI Yimin[1], TANG Siwen[2] (1. State Key Laboratory of Powder Metallurgy, Central South University, Changsha 410083, China; 2. Advanced Materials Synthesis and Application Technology Laboratory, Hunan University of Science and Technology, Xiangtan, Hunan 411201, China). p32—36

Abstract: Silicide molybdenum coating was deposited on 45 steel sbustrate with $MoSi_2$, Mo-66.7mol%Si and Mo-70 mol%Si by air plasma spraying and vacuum heat treatment. The influence of air plasma spraying and vacuum heat treatment on phase and structure evolution were studied. The results show that the phase of the coating is $MoSi_2$ and Mo_5Si_3 sprayed with $MoSi_2$ as raw material powder. The $MoSi_2$ phase were made of metastable $MoSi_2$(h) and steady $MoSi_2$(t). However, the phases of coatings are made of simple Mo and Si phases sprayed with Mo-66.7mol%Si and Mo-70mol%Si as powder respectively. The silicide molybdenum coating was not formed during plasma spraying process. The major phase is Mo_5Si_3 and minor phase is $MoSi_2$ after vacuum heat treatment at 1 050 ℃ and 1 200 ℃ for 1 h. Mo-70mol%Si coating formed a small amount of $MoSi_2$, Mo_5Si_3 and Mo_3Si phases treated at 1 050 ℃ and 1 200 ℃ for 30 min. At 1 050 ℃, with the increasing time, the relative content of $MoSi_2$ gradually increased. The diffusion reaction among

Mo, Si and Fe formed FeMoSi and Fe_3Si phases with heat treatmeat for 30 or 45 min.

Key words: plasma spraying; vacuum heat treatment; $MoSi_2$ coating; facies evolution

Wettability of lead-free solders of Sn-Zn-*x*Al CHEN Wenxue, XUE Songbai, WANG Hui, HU Yuhua (School of Materials Science and Technology, Nanjing University of Aeronautics and Astronautics, Nanjing 210016, China). p37—40, 44

Abstract: At different temperatures, the wettability of lead-free solders of Sn-9Zn-*x*Al was tested by means of wetting balance method in air and N_2 atmospheres. Effects of addition of Al, atmosphere and temperature on the wettability of lead-free solders of Sn-Zn-*x*Al were studied. The results indicate that with the addition of Al, the wettability of Sn-9Zn lead-free solders is improved obviously. With the $ZnCl_2$-NH_4Cl flux, the optimal addition of Al is about 0.02wt.%, and with the non-cleaning flux, the optimal addition of Al is about 0.005wt.%. In N_2 atmosphere, the wettability of solder on Cu substrate was extremely improved because the surface tension of the Cu substrate increases and the oxidation of the solders decreases, the surface tension of the solders decreases. With the increase of the temperature, from 215 ℃ to 245 ℃, the wettability of the solders is improved due to the decrease of the surface tension of the solders.

Key words: lead-free solder; Sn-Zn; Al; wettability; nitrogen

Upper limit of coated amorphous foils explosive welding SUN Yuxin[1,2], FU Yanshu[1], LI Qiang[1,2], WANG Jinxiang[1], ZHANG Xiaoli[1] (1. National Key Laboratory of Transient Physics, Nanjing University of Science and Technology, Nanjing 210094, China; 2. The 27th Research Institute of CETC, Zhengzhou 450000, China). p41—44

Abstract: The temperature field of foil explosive welding was simplified to one dimension non-steady heat conduction, the temperature of welding interfaces was given and changed with time. With introduction of the thermo-softening model at welding interfaces and according to the time of the tensile wave arrived at the interface, the binding strength can be confirmed. Analyses indicate that the material crystallized limit and binding strength of coating material with based metal and welding interface are the most important factors, which control the upper limit of explosive welding. The Fe-based amorphous foil coated with copper was researched. During the experiment designing, ideas of damage mechanics were used to set defects to accelerate the decaying of tensile wave. The relationship between the tensile wave strength and impact velocity was simulated by LS-DYNA, then the three upper limits were cacluclated by the important factors, and the minimum of them was the upper limits.

Key words: explosive welding upper limits; tensile wave; thermo-softening; interface strength

Analysis of interfacial fracture of resistance spot welding of dual-phase steels ZHANG Xiaoyun, ZHANG Yansong, LAI Xinmin, CHEN Guanlong (School of Mechanical Engineering, Shanghai Jiaotong University, Shanghai 200240, China). p45—48

Abstract: The transformed martensite of dual-phase steel during the cooling stage of spot welding can make the weld nugget very brittle and result in interfacial fracture which was inspected by destructive methods. This failure mode can reduce the static strength and fatigue life of the weld. 1.4 mm DP600 sheets were taken as an example, percentage of residual area in the whole nugget is used to evaluate the interfacial fracture magnitude. Then orthogonal test is used to analyze the influence of welding parameters on fracture magnitude. After single factor analysis, it can be concluded that the welding current is the most important factor that influence the welding magnitude. Using interaction analysis, the optimized welding parameters can be obtained. Experiments are conducted to validate that the modified welding parameters can reduce interfacial fracture magnitude effectively.

Key words: resistance spot welding; dual-phase steel; interfacial fracture; orthogonal experiment design

Preparation of Fe^{3+}/TiO_2 nanopowders by plasma spraying with liquid feedstock XU Dapeng, LEI Ali, FENG Lajun, YANG Shichuan (School of Material Science and Engineering, Xi'an University of Technology, Xi'an, 710048, China). p49—52

Abstract: TiO_2 nanopowders were modified through adding dopant material into precursor of liquid plasma spray. The powders were characterized by transmission electron microscopy (TEM), X-ray diffraction (XRD) and X-ray photoelectron spectroscopy (XPS). The results showed that iron-doped TiO_2 nanopowders can be prepared by liquid plasma spray, the prepared powders is in the range of 10—35 nm with spherical shape or near spherical shape and the powders were composed of mixed crystal of anatase and rutile when iron content is less than 2.0%, Fe^{3+} accelerates the transition from rutile phase to anatase phase and $Fe_2Ti_3O_9$ is precipitated when iron content is 10.0%. The iron doping can not cause long range waving of average crystallite size of powders. There are O, Ti, Fe and C elements in the prepared powders and the valency of Fe element is still +3.

Key words: TiO_2; iron ion doping; nanopowder; liquid plasma spray

Microstructure and mechanical properties of Monel alloy/copper explosive clad interface YANG Yang, CHEN Zhongping, LI Dahe, LIU Xiaohui (School of Materials Science and Engineering, Central South University, Changsha 410083, China). p53—56

Abstract: The Monel alloy/copper bimetal clad rod was produced with the explosive cladding technique. The microstructures and mechanical properties of the bonding interfaces were analyzed by means of optical microscope, scanning electron microscopy, energy spectrum analysis and shearing separate tests. The results showed that the smooth bonding interface was transformed to a wavy bonding interface as the explosive ratios increased. Deformation twins were